Geospecific rendering of alpine terrain

Simon Premože William B. Thompson Peter Shirley
Department of Computer Science
University of Utah [1]
Email: {premoze,thompson,shirley}@cs.utah.edu

Abstract. Realistic rendering of outdoor terrain requires both that the geometry of the environment be modeled accurately and that appropriate texturing by laid down on top of that geometry. While elevation data is widely available for much of the world and many methods exist for converting this data to forms suitable for graphics systems, we have much less experience with patterning the resulting surface. This paper describes an approach for using panchromatic aerial imagery to produce color views of alpine scenes. The method is able to remove shading and shadowing effects in the original image so that shading and shadowing appropriate to variable times of day can be added. Seasonal snow cover can be added in a physically plausible manner. Finally, 3–D instancing of trees and brush can be added in locations consistent with the imagery, significantly improving the visual quality.

1 Introduction

Sophisticated techniques exist for converting real-world elevation data into a *terrain skin* appropriate for graphical rendering [6, 9, 10, 16]. In most such systems, however, visual realism suffers because of the stylized texture maps or simplistic coloring used to pattern the terrain skin. To improve image quality, some high-end real-time visual simulators now support *geospecific texturing* in which texture maps are derived from aerial images registered to the terrain skin. Software techniques are also available for draping large aerial images over terrain data [4].

While draping aerial imagery onto a terrain skin adds a great deal of visual richness (Figure 1), visual realism still suffers in a number of important ways. Available high-resolution imagery is almost always panchromatic. Shadowing in the source imagery makes rendering views for times of day other than when the imagery was acquired problematic. Similar problems occur when simulating views at different times of year, particularly in alpine terrain when snow cover is an issue. Finally, texture mapping with aerial imagery in and of itself does not provide the fine scale three-dimensionality that is critical to perceiving a sense of scale over long distances. In the case of alpine environments, in particular, the three-dimensionality of trees is apparent even over distances of several kilometers.

The rendering shown in Figure 2 was produced by starting with the same source data as used to generate Figure 1. Using no additional data, terrain types and vegetation cover were mapped and this information was used to color the image. Existing shadows were removed and new shadows, appropriate to a different time of day, were added. Three-dimensional trees and brush were added at locations consistent with their appearance in the original aerial image. Finally, snow cover was added in locations appropriate for a particular time of year.

Fig. 1. *A traditional drape of panchromatic aerial imagery onto an elevation grid*

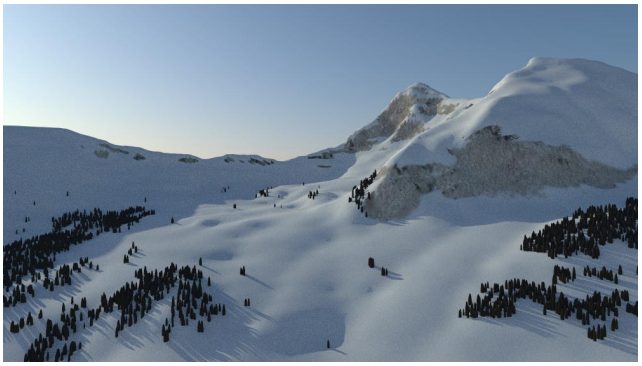

Fig. 2. *A rendering of the same data as used to generate Figure 1, after processing using the techniques from this paper.*

1.1 The nature of the data

Geospecific rendering of terrain requires information about both the geometry and the photometry of the scene. Raw information about the geometric shape of the terrain itself is most often available as a *Digital Elevation Model* (DEM), in which elevation values are represented in a rectangular grid. The highest resolution widely available elevation data for the continental U.S. are United States Geological Survey (USGS) 7.5-Minute DEMs [22]. Elevation values with a nominal precision of 1m are provided at 30m intervals (*post spacing*) on the ground. The 7.5-Minute DEMs are created by optically scanning contour maps and then fitting an approximation surface. They are subject to a number of systematic distortions that, depending on the technology used when a particular DEM was produced, can result in the actual resolvability of ground features being far worse than the 30m post spacing might suggest.

The most direct way to render geospecific photometry is to start with an image of the area to be rendered. Perspective effects make it difficult to register conventional aerial imagery with elevation data. As a result, an *orthorectification* process is often performed, in which the perspective image is warped to remove the effects of lens projection, camera orientation, and terrain. The result is an image that is effectively a scaled

orthographic projection. The USGS provides 1m resolution panchromatic (greyscale) *Digital Orthoimagery* (DOQ) for much of the continental U.S. [21]. No comparable source for color orthoimagery exists. Aerial survey companies can produce such imagery on a custom basis, but the cost is significant. Satellite images are often used to render terrain. While not true color imagery as that term is commonly used, multi-spectral satellite data can be converted to an RGB format that closely approximates perceptual color. In addition, much work has gone into the classification of multi-spectral satellite data to determine properties such as vegetation cover. Unfortunately, the resolution of available multi-spectral satellite data is at best on the order of 20m on the ground [1, 18].

If actual imagery of the terrain being rendered is to be used, the available choices are usually limited to false-colored multi-spectral satellite data of limited resolution or USGS high-resolution panchromatic orthoimagery. Since visual realism in terrain rendering depends in part on high resolution texturing, it is important to explore whether or not panchromatic orthoimagery can be effectively utilized. Can realistic color be generated? Can we get enough information about ground cover to add detail not resolved in the imagery? Can we remove shadows and shading effects so as to simulate views at times other than when the original imagery was acquired? Can we simulate seasonal effects not present in the original imagery?

1.2 System overview

We developed a modeling and rendering environment that meets the goals and considerations described above (Figure 3). Input consists of terrain elevation data and orthophoto data. These two sources of information are used as input by a pattern classification system to categorize each pixel in the image into one of a set of possible classes (e.g., rock, snow, tree, etc.). The classifier is also capable of identifying shadowed regions in the original image, together with unshadowed areas of the same class. This is sufficient to enable a deshadowing process in which shadowed areas of a given type are made to be visually similar to the corresponding unshadowed regions. The classification is also used to develop explicit geometric models for larger objects such as trees. Finally, a physically-based snow simulation is used to compute snow cover for a given date. All of these are combined to form a terrain skin covered by a colored texture map and a set of geospecific vegetation models.

The major obstacles that must be crossed to create such a system include:

- removing shadows shading effects from orthoimagery (Sections 2.1 and 2.3),
- classifying the pixels in orthoimages into categories (Section 2.2),
- adding seasonal effects (Section 3).
- add geometry for the major vegetation in the appropriate locations.

2 Normalizing and classifying orthoimages

Orthoimages are produced from conventional aerial photographs and are subject to all of the vagrancies of the photographic process. Though care is taken to use images taken when the sun angle is high, shadows still occur. This is particularly so in images of alpine terrain due to the steep slopes that are often present. To determine surface type at each location in an orthoimage, it is desirable to first reduce those brightness effects in the image that are due to shading rather than surface reflectivity. In order to render

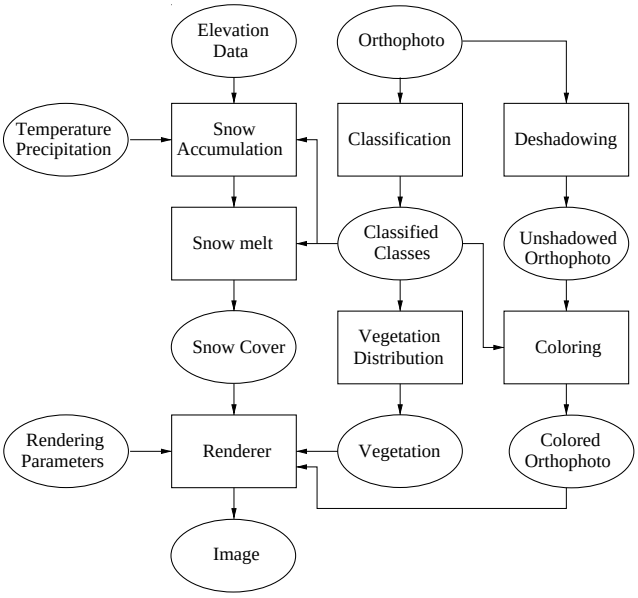

Fig. 3. Scene synthesis flow graph

a view with a simulated sun angle different from the actual sun angle when the image was required, this same shading normalization must be accompanied by a process that removes the existing shadows.

2.1 Removing shading effects

To use aerial imagery in the rendering of terrain as it would appear at different times of day, we need to minimize the luminance variability in the source imagery that is due to illumination effects at the time the imagery was acquired. If we had a way to recover surface albedo from luminance, this would also aid in determining what sort of surface cover was present at a given location in the image. Given Lambertian surfaces, a known distribution of illumination, and surface orientation at every point, it is straightforward to determine surface reflectances. In practice, we know none of these properties. Surface reflectance is far from Lambertian, illumination depends not only on sun angle but also on complex, weather dependent variations in sky brightness, and DEMs provide only low resolution information about surface orientation.

Nevertheless, shading effects can be reduced by applying a normalization based on the cosine of the angle between the approximate surface orientation, as specified in a DEM, and an estimate of the direct illumination direction. Sun angle is often provided with satellite data. For USGS orthoimages, it must be estimated from the imagery. Computer vision shape-from-shading methods can be used to solve this problem [3]. If shadows are present and one or more matches can be established between points on shadow generating contours and the corresponding point on the trailing edge of the shadow, then the direction of direct illumination can be inferred from the DEM-specified elevations of the corresponding points.

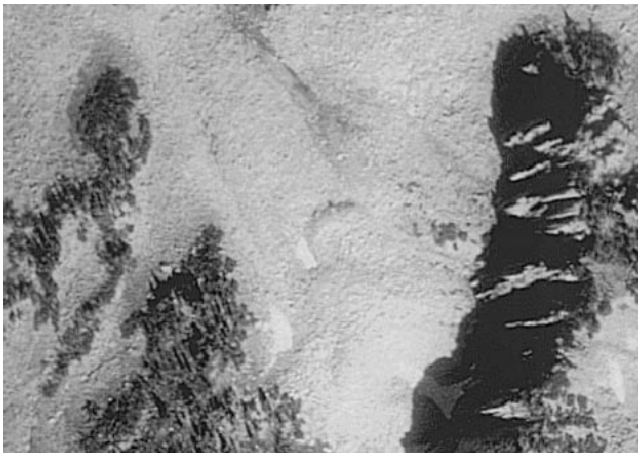

Fig. 4. *480m by 340m section of an orthoimage of the Rocky Mountains*

2.2 Classifying orthoimages

Figure 4 shows a 480m by 340m section of an orthoimage of an area of the Rocky Mountains. Included within the image are regions of pine trees, brush, talus, rock cliffs, and snow. The pine trees are surrounded by an understory consisting of dirt, grass, and shrub. Portions of talus, cliff, and snow are in shadow. Each of these classes of surface cover has a distinct coloration. Given the panchromatic brightness at each pixel and the corresponding surface type, it is straightforward to produce a relatively accurate color version of the image.

Image brightness can yield a rough categorization of these regions: pine is dark, talus a mid-gray, and snow is bright. A quantitative examination of image values, however, quickly demonstrates that thresholding cannot adequately separate the classes of interest, no matter how carefully the thresholds are chosen. Computer vision techniques based on 2–D shape analysis are not likely to succeed either, given the complexity of the images. Instead, we have successfully used a pattern classification approach similar to that used to classify multi-spectral satellite data.

For each pixel in the deshaded orthoimage, we computed eight features:

1. pixel brightness
2. average neighborhood brightness
3. minimum neighborhood brightness
4. maximum neighborhood brightness
5. elevation
6. slope
7. aspect
8. angle to southern occluder

Features 2–4 allow consideration of brightness within a local context. Features 5–8 are computed by interpolating 30m DEM values. Feature 7 measures the direction a given point on a slope is facing, and important determinant of vegetation cover. Feature 8 measure the angle from a given point to the southern skyline. Larger values increase the likelihood that the point will be in shadow when the image was acquired.

A simple normal distribution, maximum likelihood Bayes classifier [20] proved sufficient, avoiding the need for complex training procedures, hand tuning of parameters, or other manual adjustments. This classifier assumes that the values of each feature for each class are generated by a normally distributed random process, possibly involving correlation between different features. Population statistics, $p(\mathbf{x}|C_k)$, are computed for feature values, represented as a vector $\mathbf{x}$, given that the features came from a particular class, C_k. Since the feature values arising from a given class are assumed to be normally distributed, their statistics are completely characterized by a mean vector, μ_k, and a covariance matrix, Φ_k. It is easily shown that given the *a priori* likelihood of each class, $P(C_k)$, the minimum error classifier is achieved by assigning the class C_k such that:

$$P(C_k|\mathbf{x}) \geq P(C_j|\mathbf{x}) \; \forall \; j \neq k$$

Bayes law is used to convert this to a discriminant function formulation, in which C_k is chosen maximizing:

$$g_k = -\frac{1}{2}\mathbf{x}^t[\Phi_k]^{-1}\mathbf{x} + \mathbf{x}^t[\Phi_k]^{-1}\mu_k - \frac{1}{2}\mu_k^t[\Phi_k]^{-1}\mu_k + \ln P(C_k) - \frac{1}{2}\ln|\Phi_k|$$

For each class, several hundred image locations were selected manually to form a training set, in a process requiring only a few minutes of time. Statistics on the distributions of feature values for the training set were determined and used to form the discriminant functions for the maximum likelihood Bayes classifier, assuming all *a priori* probabilities to be equal. This classifier was then used to categorize each pixel location in the full orthoimage. A final decluttering step reclassified very small regions based on the dominant surrounding class.

Classification results are shown in Figure 5. While ground-truth validation has not been done, spot checking of the results corresponds closely with what would be expected from a careful examination of the orthoimage. The actual statistical distribution characterizing the features is almost certainly not multi-variate normal. The fact that the classifier still performed well is an indication that the features for each class are well separated in a statistical sense. As is often the experience in pattern recognition, appropriately chosen features allowed the use of a simple classifier.

2.3 Removing shadows

While the aerial imagery used to generate orthoimages is chosen to minimize shadows, shadowing is still present. As would be expected, the severity of this problem increases with the ruggedness of the terrain. These shadows need to be removed and replaced by simulated shadows resulting from a different illumination direction if we want to use the imagery to texture a terrain scene for a date/time different from when the source image was taken. Given accurate information about the direction of incident direct illumination and high resolution elevation data, expected shadow locations could be easily computed. In practice, we seldom have either and so another approach is needed.

The maximum likelihood classifier does a good job of identifying shadow areas and can even categorize different surface covers within the shadowed regions. This can be used to remove the photometric effects of shadowing, even when the direction of illumination is not known. For purposes of visual rendering, it is enough to renormalize shadowed portions of the orthoimage to have a brightness distribution statistically

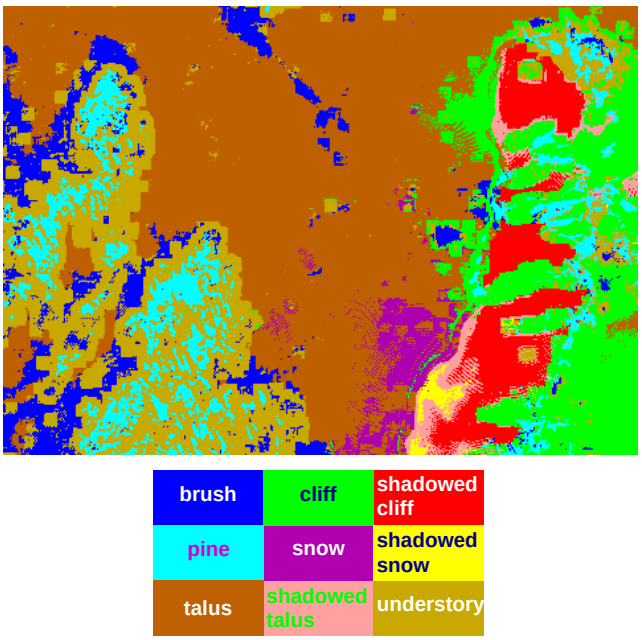

Fig. 5. *Classification results*

similar to unshadowed regions of the same surface type. In practice, it appears to be enough to standardize the mean and standard deviations of the shadowed regions. To improve the visual qualities of our talus texture, we apply image processing. The real talus exhibits shadowing and highlights from individual stones. Most of this is lost in the blurring of the photographics process. To add some shading variation, we apply two steps. First, we apply mean-variance normalization. Because the dynamic range in the shadows is so low, the variance normalization effectively translates quantization noise into uncorrelated additive noise. We then apply a gaussian blur, thus adding correlation to the noise for an appearance that more resembles the mid-size rocks of talus.

Often, shadow boundaries in orthoimages exhibit a penumbra-like effect, though at a scale much larger than the shadow penumbra that would be generated by a light source the angular extent of the sun. The causes of this phenomenon are not clear, but are likely due to a combination of interreflection, variations in sky brightness, and photographic dodging done as a pre-processing step in orthophoto preparation. Whatever the cause, these shadow fringes are visually distracting and can generate ground type misclassifications. Fortunately, it is an easy matter to replace dark pixels near classified shadow regions with lighter pixels slightly farther away, largely eliminating the problem.

Figure 6 shows the results of deshading and shadow removal applied to Figure 4 and followed by coloring based on the classification shown in Figure 5.

3 Modeling snow cover

In alpine environments, snow cover is the predominant seasonal effect. Snow cover normally develops from a series of winter storms and is modified by the action of rain,

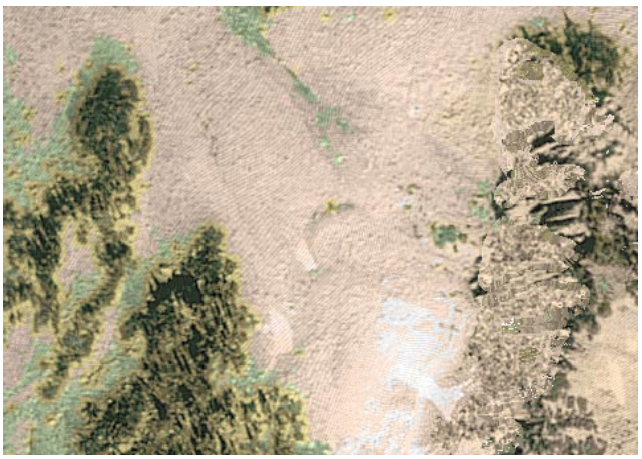

Fig. 6. *Figure 4 deshaded, colored, and with shadows removed*

wind and melting. Thus, to show seasonal effects not present in the original orthoimagery, we need to simulate effects such as snow accumulation, snow ablation and melt. In mountainous areas, the amount of snow present at any given location is highly variable. This is particularly noticeable in late spring and early summer, as southern and western aspects melt out exposing the underlying ground, while north facing slopes are still covered in deep snow.

3.1 Snow accumulation

Snow accumulation and loss is controlled primarily by atmospheric conditions and the elevation and slope of the terrain [8]. Atmospheric processes of interest are precipitation, deposition, condensation, turbulent transfer of heat and moisture, radiative exchange and air movement. Land features influence snow accumulation by slope, orientation, and by shadowing properties. These factors act together and are related to each other [2]. For example, mountain ranges interrupt the winds that can redistribute the snow into drifts, slope and aspect influence incoming solar radiation and humidity, and latitude and elevation control air and ground temperature.

The variability of snow cover is commonly considered on three geometric scales [8]:

- *Regional scale*: large areas with linear distances up to 1000km in which dynamic meteorological effects such as wind flow around barriers and lake effects are important
- *Local scale*: areas with linear distances of 100m to 1000m in which accumulation may be related to the elevation, aspect and slope of the terrain and to the canopy and crop density, tree species, height and extent of the vegetative cover
- *Microscale*: distances of 10m to 100m over which accumulation patterns result primarily due to surface roughness

For our simulations, we consider only local scale and microscale.

3.2 Snow ablation and melt

The rate of snow melt is dependent on energy availability, which is mostly in the form of radiation [12]. Cold snowpacks have a negative energy balance, but warming causes the snowpack to become isothermal (0^oC) and additional energy results in positive energy balance and melt. Daily snow melt in forested areas is considerably less than melt in open areas, as forests protect the snow cover from solar radiation and wind. Canopy warming can increase longwave radiation, but the net effect of forest is reduction in melt. Rain falling on snowpack may accelerate its melt rate, but intense sunshine of late spring and summer is the principal melting energy source.

Most operational procedures for snow melt prediction rely on ambient air temperature as the index of the energy available for melt. The *temperature index* is usually used to characterize the level of the energy balance because it is superior to other simple methods for the full energy balance at the snow surface [5]. The most common expression relating snow melt to the temperature index is:

$$M = C_m(T_{air} - T_{melt}),$$

where M is the daily snow melt (mm/day), C_m is the melt rate factor (mm/^oC per day), T_{air} is the daily ambient temperature (^{o}C) and T_{melt} is the threshold melt temperature (^oC). The critical melt temperature is often set to 0 ^oC but can be optimized for a particular location.

3.3 Snow cover simulation

Our model divides the height field into a grid storing the amount of snow as *snow water equivalent*. This is the mass of water stored as snow per m^2. Snow is first deposited by elevation and then is melted in a simulation that varies temperature with height and available radiation. The available radiation is based on surface orientation and the times of day it is shadowed. The shadowing is computed at the center of each grid cell.

Ambient air temperature is a fundamental component of the calculations for snow accumulation, melt and evapotranspiration. Temperature data at specified base elevation is provided as user input and contains: (i) minimum, (ii) maximum, and (iii) average temperature. An average environmental lapse rate can also be user specified, but we adopted a rate of -0.6^oC per 100m [14]. Warm air advection can make a standard lapse rate inadequate for temperature predictions in alpine environment [17]. However, over time fluctuations about the mean lapse rate will tend to even out.

Elevation is believed to be the single most important factor in snow cover distribution. Precipitation data at specified base elevation is provided as user input and contains: (i) amount of precipitation, and (ii) precipitation density (1 g/cm^3 for rain). Elevation rise from the base elevation is treated very simply using an optional user specified lapse rate. As with air temperature, the simplified precipitation distribution assumptions are less likely to pose problems over long time periods.

The amount of snow accumulated depends on the balance between rain and snowfall [17]. The usual method to classify precipitation is to set a threshold ambient air temperature (T_{snow}) above which all precipitation is assumed to be rain. For every simulation time step, we determine precipitation type from ambient air temperature. If precipitation is snow, the snow water equivalent is computed from snowfall and density, and accumulated. If precipitation is rain no accumulation occurs and the simulation continues to melting phase.

The major variables controlling the snow melt factor are determined using the rela-

tionship suggested by Eggleston et al. [13]:

$$C_m = k_m k_v R_I (1 - A)$$

where k_m is a proportionally constant, k_v is a vegetation transmission coefficient for radiation, R_I is a solar radiation index, and A is the snow albedo. The change in snow albedo with time t (days) is described by

$$A = 0.4[1 + e^{-k_e t}]$$

where k_e ($\approx 0.2/day$) is a time constant. A fall of new snow increases the albedo to 0.8 while rain reduces it to 0.4. The vegetation transmission coefficient k_v is computed as

$$k_v = e^{-4C_v}$$

where C_v is the vegetation canopy density.

R_I is the ratio of the radiation received by a surface with a given slope and aspect, normalized to that received by a horizontal surface at the same latitude and time of year. Note that only the ratio of energies needs to be computed. A slightly modified method of Swift [19] is used for this computation. For periods of rain the melt factor C_m is adjusted as follows:

$$C_m(rain) = C_m + 0.00126 P_{rain}$$

where P_{rain} is amount of rainfall (mm).

Every simulation time step, if the ambient air temperature (T_{air}) is greater than the threshold melt temperature (T_{melt}), the melt rate factor C_m is computed and the snowpack water equivalent is adjusted accordingly. When the simulation is done, grid cells with non-zero snow water equivalent are assumed to have snow cover. We do not model snow depth so we use the snow cover information only to decide where to render snow in the final image. Adding snow to regions that are uncovered in the original orthoimage is straightforward, since at a distance snow appears as a relatively diffuse reflector except for glancing illumination and viewing angles. Subtracting snow that was on the ground when the aerial image was shot is a bit more complicated. However, since almost all of the raw imagery is acquired in summer to minimize sun angle effects, we can be pretty much assured that the underlying surface cover is rock or talus.

4 Results

Figures 7–9 show renderings produced for a 2km by 2km region in the Rocky Mountains. This particular region was selected because it includes both rugged and fairly gentle terrain, significant shadowing, a fairly wide range of surface types, and slopes of varying aspect, all within a relatively compact area. The sole source data utilized was standard issue USGS DEM elevation and DOQ image data. A classification map was created as described in Section 2.2. This was used for deshadowing, coloring, and for seeding a plant growth simulation in the manner of Deussen et al. [15], with the individual plants represented using ellipsoids in the spirit of Gardner [7]. For a given time of year, a snow simulation is run and the appropriate parts of the colored orthotexture are replaced with snow color. The texture and plant data was input to a Monte Carlo path tracer [11] with a sky model similar to that used by Yu et al. [23] that appropriately controls illumination based on time/date/place.

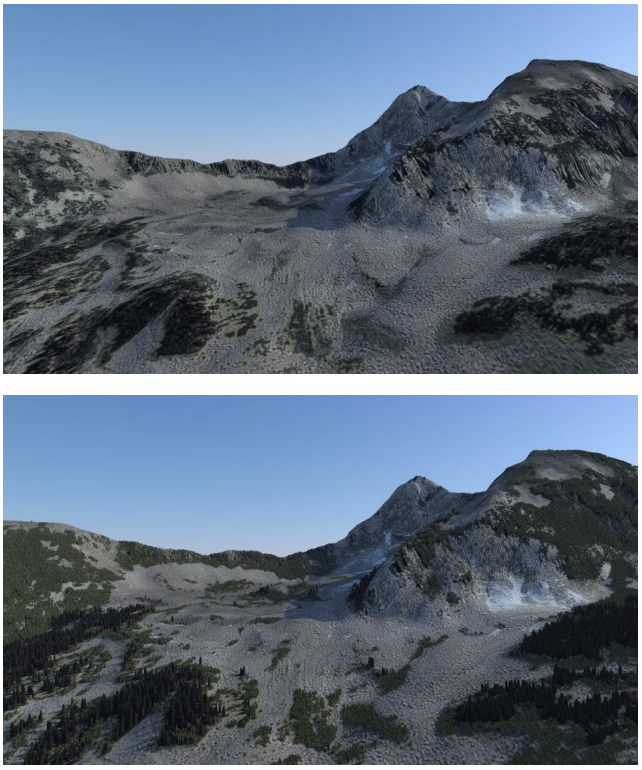

Fig. 7. *Image with and without explicit tree/brush geometry.*

Figure 7 shows renderings with and without explicit plant geometry. Figure 8 shows variation of appearance at different times of day. Figure 9 shows variation of appearance at different times of year. Figure 9 shows variations due to seasonal effects.

References

1. AERIAL-IMAGES, INC. http://www.aerial-images.com. 615 Hillsborough Street, Raleigh, NC 27603, USA.
2. BARRY, R. G. *Mountain Weather and Climate*. Methuen, London, UK, 1981.
3. BROOKS, M. J., AND HORN, B. K. P. Shape and source from shading. In *Shape from Shading*, B. K. P. Horn and M. J. Brooks, Eds. MIT Press, Cambridge, MA, 1989.
4. CLINE, D., AND EGBERT, P. Interactive display of very large textures. In *Proceedings of IEEE Visualization '98* (Oct. 1998), pp. 343–350.
5. FERGUSON, R., AND MORRIS, E. Snowmelt modelling in the Cairngorms. *Earth Sci.*, 78 (1987), 261–267.
6. FOWLER, R. J., AND LITTLE, J. J. Automatic extraction of irregular network digital terrain models. In *SIGGRAPH 79 Conference Proceedings* (1979), Annual Conference Series, ACM SIGGRAPH, pp. 207–218.
7. GARDNER, G. Y. Simulation of natural scenes using textured quadric surfaces. In *Computer Graphics (SIGGRAPH '84 Proceedings)* (July 1984), H. Christiansen, Ed., vol. 18, pp. 11–20.

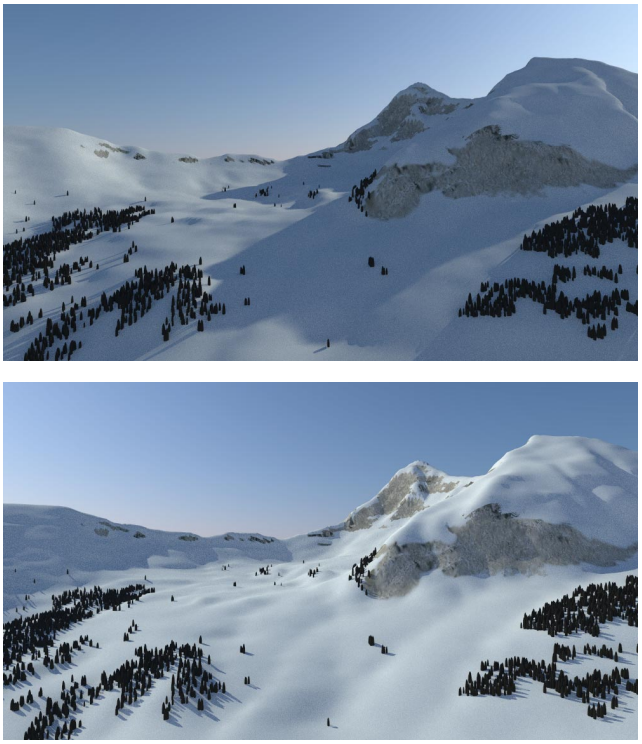

Fig. 8. *Renderings for winter morning and afternoon.*

8. GRAY, D. M., AND MALE, D. H., Eds. *Handbook of Snow*. Pergamon Press, 1981.
9. HOPPE, H., DEROSE, T., DUCHAMP, T., MCDONALD, J., AND STUETZLE, W. Mesh optimization. In *Computer Graphics (SIGGRAPH '93 Proceedings)* (Aug. 1993), J. T. Kajiya, Ed., vol. 27, pp. 19–26.
10. HOPPE, H. H. Smooth view-dependent level-of-detail control and its application to terrain rendering. In *Proceedings of IEEE Visualization '98* (Oct. 1998), pp. 343–350.
11. KAJIYA, J. T. The rendering equation. In *Computer Graphics (SIGGRAPH '86 Proceedings)* (Aug. 1986), D. C. Evans and R. J. Athay, Eds., vol. 20, pp. 143–150.
12. KELLY ELDER, J. D., AND MICHAELSEN, J. Snow accumulation and distribution in an alpine watershed. *Water Resources Research 27*, 7 (1991), 1541–1552.
13. K.O. EGGLESTON, E. I., AND RILEY, J. Hybrid computer simulation of the accumulation and melt processes in a snowpack. Technical Report PRWG65-1, Utah State University, Logan, UT, USA, 1971.
14. LEEMANS, R., AND CRAMER, W. The HASA climate database for mean monthly values of temperature, precipitation and cloudiness on a terrestrial grid, 1991. RR-91-18, HASA, Laxenburg.
15. OLIVER DEUSSEN, PAT HANRAHAN, BERND LINTERMAN, RADOMIR MĚCH, MATT PHARR AND PRZEMYSLAV PRUSINKIEWICZ. Realistic modeling and rendering of plant ecosystems. In *SIGGRAPH 98 Conference Proceedings* (July 1998), pp. 275–286.
16. POPE, C. N., VUONG, M., MOORE, R. G., AND COWSER, S. S. A whole new CCTT world. *Military Simulation and Training*, 5 (1995).
17. ROHRER, M. Determination of transition air temperature from snow to rain and intensity of precipitation. In *WMO IASH ETH International Workshop on Precipitation Measurement*

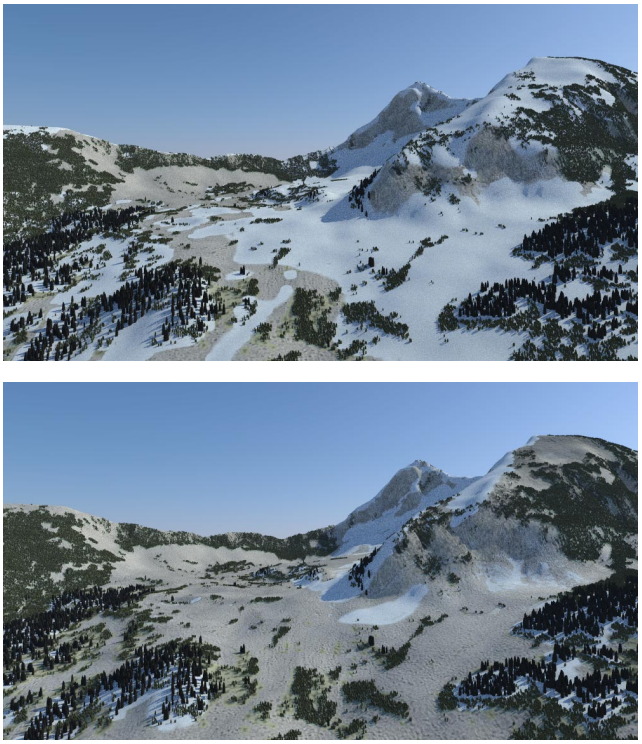

Fig. 9. *Renderings for early and late spring.*

(Oct. 1989), pp. 475–582.
18. SPOT IMAGE CORPORATION. http://www.spot.com. 1897 Preston White Drive, Reston, VA 20191, USA.
19. SWIFT, L. W. Algorithm for solar radiation on mountain slopes. *Water Resources Research 12*, 1 (1976), 108–112.
20. TOU, J. T., AND GONZALEZ, R. C. *Pattern Recognition Principles*. Addison-Wesley, Reading, MA, 1974.
21. U.S. GEOLOGICAL SURVEY. Standards for digital orthophotos, December 1996.
22. U.S. GEOLOGICAL SURVEY. Standards for digital elevation models, January 1998.
23. YU, Y., AND MALIK, J. Recovering photometric properties of architectural scenes from photographs. In *SIGGRAPH 98 Conference Proceedings* (July 1998), M. Cohen, Ed., Annual Conference Series, ACM SIGGRAPH, Addison Wesley, pp. 207–218.